Three-phonon phase space and lattice thermal conductivity in semiconductors

2008 J. Phys.: Condens. Matter 20 165209

(http://iopscience.iop.org/0953-8984/20/16/165209)

IOP PUBLISHING JOURNAL OF PHYSICS: CONDENSED MATTER

J. Phys.: Condens. Matter **20** (2008) 165209 (6pp) doi:10.1088/0953-8984/20/16/165209

Three-phonon phase space and lattice thermal conductivity in semiconductors

L Lindsay and D A Broido

Department of Physics, Boston College, Chestnut Hill, MA 02467, USA

Received 25 January 2008, in final form 10 March 2008
Published 31 March 2008
Online at stacks.iop.org/JPhysCM/20/165209

Abstract

We present calculations of the phase space for three-phonon scattering events in several group IV, III–V and II–VI semiconductors employing an adiabatic bond charge model to accurately represent the phonon dispersions. We demonstrate that this phase space varies inversely with the measured lattice thermal conductivities of these materials over a wide range of temperatures where three-phonon scattering is the dominant mechanism for scattering phonons. We find that this qualitative relationship is robust in spite of variations in material parameters between the semiconductors. Anomalous behavior occurs in three III–V materials that have large mass differences between constituent elements, which we explain in terms of the severely restricted three-phonon phase space arising from the large gap between acoustic and optic phonon branches.

1. Introduction

A material's lattice thermal conductivity is an essential component in determining its potential utility for thermal management applications. Among these are the development of materials that facilitate heat dissipation in microelectronics and nanoelectronics [1] and that provide efficient thermoelectric refrigeration and power generation [2].

Above a few tens of degrees kelvin, the lattice thermal conductivity of high-quality crystalline semiconductors is determined primarily by phonon–phonon scattering [3, 4] which arises when atoms in the lattice deviate sufficiently from their equilibrium positions that they sample the anharmonicity of the interatomic potential. Other extrinsic scattering mechanisms, such as due to isotopic impurities and boundaries, are significantly less important in this temperature range [4]. The lowest order anharmonic terms correspond to three-phonon scattering processes. Around room temperature, these processes are stronger than the higher order anharmonic scattering processes [5] and thus dominate the behavior of the lattice thermal conductivity.

It has been noted some time ago that, in the temperature range where three-phonon scattering is dominant, an inverse relationship should exist between the phase space for three-phonon scattering (defined below) and the intrinsic lattice thermal conductivity of a material [3]. While other material parameters such as averaged acoustic phonon velocity, Grüneisen constant, heat capacity and density, are often used in simple-model estimates of the lattice thermal conductivity [3, 4], to date, no calculations have been performed that compare a material's three-phonon phase space to measured lattice thermal conductivities. In this paper, we perform such calculations. Specifically, we calculate the three-phonon phase space for several group IV, III–V and II–VI semiconductors.

The three-phonon phase space is determined entirely from a material's phonon dispersion, and these dispersions have been precisely measured for many materials. We calculate these phonon dispersions accurately using an adiabatic bond charge model [6, 7]. We show that the three-phonon phase space indeed varies inversely with the measured thermal conductivities of the studied materials over a wide range of temperatures. Furthermore, we find that this qualitative relationship is maintained in spite of the dependence of the thermal conductivity on other material parameters. Finally, we find that several III–V materials having large mass ratios of the constituent atoms possess anomalously small phase spaces for three-phonon scattering. This results from the large frequency gaps between acoustic and optic phonon branches, which freezes out three-phonon scattering processes involving acoustic and optic phonons. We connect this anomalously small phase space to a corresponding enhancement in the thermal conductivity, behavior that has been noted qualitatively many years ago [8].

Section 2 presents the theory for calculating the three-phonon phase space. In section 3, the calculated three-phonon phase spaces for different materials are compared to corresponding measured thermal conductivities and an

Table 1. Shown here are the semiconductors examined in this paper as well as their corresponding lattice thermal conductivities for temperatures $T = 300$ K and 150 K, mass ratios, and gaps between acoustic and optic branches as determined by the adiabatic bond charge model [6, 7]. The total phase space for three-phonon scattering, P_3, is also given here for comparison.

	$\kappa_{\text{exp},T=300\text{ K}}$ (W cm^{-1} K^{-1})	$\kappa_{\text{exp},T=150\text{ K}}$ (W cm^{-1} K^{-1})	$m_>/m_<$	Gap (THz)	P_3 (10^{-2})
Si	1.53[a]	4.78[a]	1	0	0.3536
Ge	0.70[b]	1.71[b]	1	0	0.5795
C	32[c]	149[c]	1	0	0.0796
GaAs	0.45[d]	1.06[d]	1.07	0.04	0.6015
GaSb	0.36[d]	0.78[d]	1.75	0.59	0.6605
GaP	1.10[e]	2.13[e]	2.25	3.14	0.3360
InP	0.68[f]	1.90[f]	3.71	3.80	0.3822
InSb	0.166[d]	0.40[d]	1.06	0.07	0.7230
AlSb	0.60[e]	1.05[e]	4.51	4.30	0.2641
CdTe	0.075[g]	0.184[g]	1.14	0.31	0.9424
ZnTe	0.18[h]	0.45[h]	1.95	0.38	0.8528

[a] Reference [10]. [b] Reference [11].
[c] Reference [12]. [d] Reference [13].
[e] Reference [14]. [f] Reference [15].
[g] Reference [16]. [h] Reference [17].

understanding of the observed behavior is developed. Section 4 provides a summary and conclusions.

2. Theory

We consider scattering between three phonons in modes, $(j, \mathbf{q})$, $(j', \mathbf{q}')$ and $(j'', \mathbf{q}'')$. Here, $\mathbf{q}, \mathbf{q}'$ and $\mathbf{q}''$ are the momenta of the three phonons and j, j' and j'' designate the phonon branches. The three-phonon scattering processes are constrained to satisfy energy and momentum conservation:

$$\omega_j(\mathbf{q}) \pm \omega_{j'}(\mathbf{q}') = \omega_{j''}(\mathbf{q}''), \qquad \mathbf{q} \pm \mathbf{q}' = \mathbf{q}'' + \mathbf{G}. \quad (1)$$

Here $\omega_j(\mathbf{q})$ is the phonon frequency of mode $(j, \mathbf{q})$, $\mathbf{G}$ is a reciprocal lattice vector that is zero for normal processes and non-zero for umklapp processes, and the $\pm$ signs correspond to the two types of possible three-phonon processes [3, 4]. Equation (1) impose severe constraints on the phase space available for three-phonon scattering.

We consider a reciprocal lattice with n_j phonon branches whose Brillouin zone has volume, V_{BZ}. We define the total phase space available for three-phonon processes, normal and umklapp, as the sum over all possible modes for three phonons subject to the constraints of equation (1):

$$P_3 = \frac{2}{3\Omega}\left(P_3^{(+)} + \frac{1}{2}P_3^{(-)}\right) \quad (2)$$

where

$$P_3^{(\pm)} = \sum_j \int \mathrm{d}\mathbf{q} D_j^{(\pm)}(\mathbf{q}) \quad (3)$$

and

$$D_j^{(\pm)}(\mathbf{q}) = \sum_{j',j''} \int \mathrm{d}\mathbf{q}' \delta(\omega_j(\mathbf{q}) \pm \omega_{j'}(\mathbf{q}') - \omega_{j''}(\mathbf{q} \pm \mathbf{q}' - \mathbf{G})) \quad (4)$$

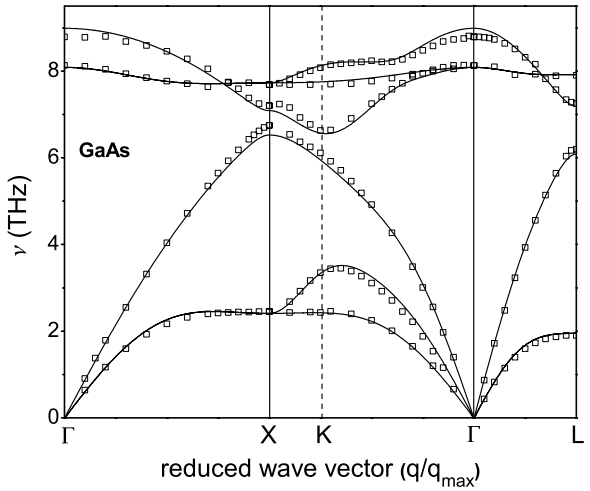

Figure 1. Phonon dispersion of GaAs. Solid lines are calculated results using the abcm. Open squares are given by neutron scattering data from [18].

where the integration in equations (3) and (4) is taken over the first Brillouin zone. The quantity, $\Omega = n_j^3 V_{\text{BZ}}^2$, is a normalization factor equal to the unrestricted phase space for each type of process. This choice along with the additional 2/3 factor gives $P_3 = 1$ when the energy-conserving delta function in equation (4) is removed. The factor of 1/2 in equation (2) arises to prevent double-counting of scattering events [3, 4]. We note that using the symmetry of the delta function, it is straightforward to show that $P_3^{(+)} = P_3^{(-)}$, so only one of these need be calculated explicitly and, from equation (2), $P_3 = P_3^{(+)}/\Omega$. In equations (3) and (4), $D_j^{(\pm)}(\mathbf{q})$ is the two-phonon density of states [9] and momentum conservation has already been imposed on $\mathbf{q}''$. For umklapp processes the $\mathbf{G}$ vectors that enter equation (4) are the eight shortest and six second-shortest vectors for the truncated octahedron Brillouin zone corresponding to the real space FCC lattice.

We focused our study on three-phonon scattering in group IV, III–V and II–VI bulk semiconductors with diamond or zincblende structure and in a temperature range between 150 K and room temperature, $T = 300$ K, where three-phonon scattering dominates the thermal resistivity. A list of the materials examined here with corresponding properties relevant to later discussion is given in table 1. To accurately describe the phonon frequencies that enter the calculation of the allowed three-phonon scattering phase space in each material, we employed an adiabatic bond charge model (abcm), introduced by Weber [6, 7]. This model accurately reproduces experimental phonon dispersion data including anisotropies and the characteristic flattening of the transverse acoustic branches near the Brillouin zone boundary observed in many semiconductors. An example of this is provided for GaAs in figure 1. For the II–VI materials, we used a modification of the abcm as described in [19].

To obtain the best set of abcm parameters, we implemented a χ^2 minimization procedure for each material, with χ^2 defined as [20]:

$$\chi^2 = \sum_{j,\mathbf{q}} (\omega_j^{\text{abcm}}(\mathbf{q}) - \omega_j^{\text{exp}}(\mathbf{q}))^2. \quad (5)$$

Table 2. Best fit parameters to experimental dispersion data for the adiabatic bond charge model. These choices for parameters were guided solely by their fit to the available data so that the calculated P_3 in each material is as accurate as possible.

	$\frac{1}{3}\phi''_{i-i}$	$\frac{1}{3}\phi''_{i_1-bc}$	$\frac{1}{3}\phi''_{i_2-bc}$	β_1	β_2	Z^2/ε
Si	6.21	6.47	6.47	8.60	8.60	0.180
Ge	6.25	9.57	9.57	7.88	7.88	0.279
C[a]	−10.1	51.0	51.0	12.6	12.6	0.885
GaAs[a]	5.24	5.85	32.5	2.48	10.4	0.392
GaSb[a]	6.95	2.60	16.2	4.34	7.57	0.192
GaP[a]	3.76	8.67	65.5	−2.02	33.7	0.589
InP[a]	1.32	19.6	102	0.409	13.3	1.06
InSb	7.32	2.15	14.7	3.59	10.3	0.173
AlSb	5.13	7.92	37.5	−0.756	28.0	0.462
CdTe[b]	6.85	0.77	23.3	0.39	15.4	0.183
ZnTe[b]	5.51	1.06	22.9	1.07	17.0	0.180

[a] Additional parameters, a' and $\frac{1}{2}(\psi''_1 - \psi''_2)$, defined in [6] and [7], were used for these materials in order to maximize the fit to experimental data: $a' = (0.49, 0.89, 2.49)$ in (C, GaP, InP); $\frac{1}{2}(\psi''_1 - \psi''_2) = (3.52, 1.08, 1.62, 3.35)$ in (GaAs, InP, GaSb, InSb), respectively.

[b] Parameters from [19].

Here, $\omega_j^{\text{abcm}}(\mathbf{q})$ and $\omega_j^{\text{exp}}(\mathbf{q})$ are the calculated and measured phonon frequencies, and the sum is over the set of $(j, \mathbf{q})$ obtained from available experimental data. The parameter sets providing the minimum χ^2 for each material are shown in table 2.

The phase space calculation was performed numerically using two separate methods, direct integration and the tetrahedron method [21]. The first involved direct integration over $\mathbf{q}$ and $\mathbf{q}'$ in equations (3), and (4). For each $\mathbf{q}$ and set of branch indices, (j, j', j''), the conservation conditions, equation (1), represent four constraint equations in a 6-dimensional $(\mathbf{q}', \mathbf{q}'')$ momentum space. The remaining two degrees of freedom define a two-dimensional surface in $\mathbf{q}'$ for each type of process (+ or −). The direct integration method utilized a root-finding scheme to approximate these surfaces for each, $(j, j', j'', \mathbf{q})$. In the tetrahedron method [21], which is often used in density of states calculations, equation (4) is evaluated by dividing the Brillouin zone into tetrahedra that fill the entire reciprocal space. Linearly interpolated expressions for the frequencies within each tetrahedron are determined from the exact frequencies calculated at the vertices using the abcm. Both methods gave results for the total three-phonon scattering phase space within 4% of each other for every material, though the tetrahedron method converged with much less computational effort.

3. Results and discussion

Figure 2 shows the calculated phase space for three-phonon scattering, P_3, plotted against the measured room temperature (300 K) lattice thermal conductivity for each group IV, III–V and II–VI semiconductor listed in table 1. It is evident from this figure that P_3 varies inversely with the lattice thermal conductivity. This makes physical sense: as P_3 decreases from material to material, the reduced phonon scattering corresponds to an increase in the thermal conductivity.

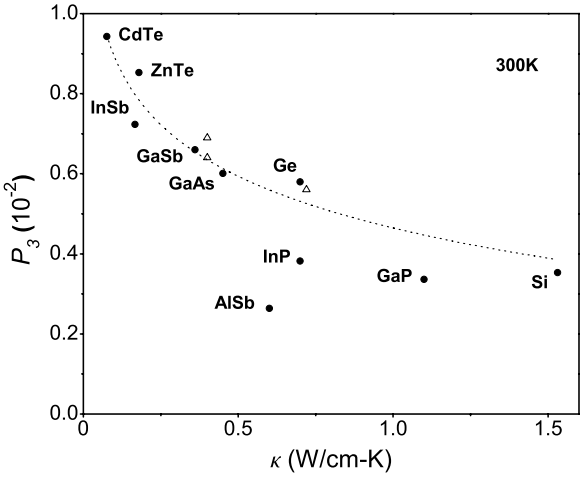

Figure 2. Three-phonon scattering phase space versus measured lattice thermal conductivity at $T = 300$ K (references in table 1) for a host of semiconductors. Triangles correspond to hypothetical values for anomalous materials, InP, AlSb, and GaP.

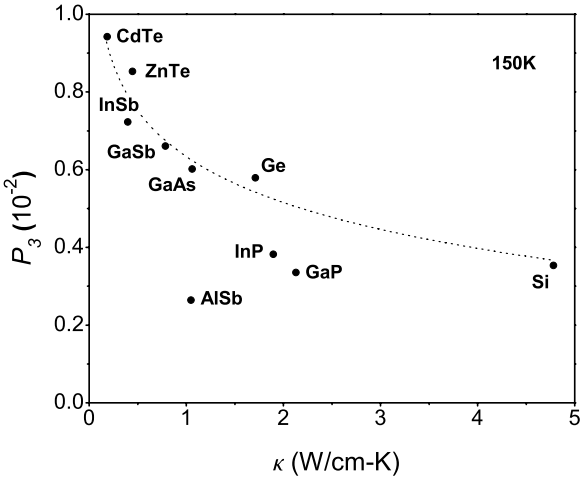

Figure 3. Three-phonon scattering phase space versus measured lattice thermal conductivity for the same materials as in figure 2 (references in table 1) but with $T = 150$ K. Note the different scale along the horizontal axis as compared to figure 2.

Materials such as cadmium telluride with a relatively large P_3 have a low lattice thermal conductivity while silicon and diamond with small P_3 have correspondingly high lattice thermal conductivities.

Figure 3 shows the three-phonon phase space versus measured lattice thermal conductivity values for 150 K. It is evident that an inverse relationship between three-phonon phase space and thermal conductivity also occurs for the lower temperature case, but with all points shifted to the right (to higher thermal conductivity). We have investigated results for other temperatures between 150 and 300 K and find the same qualitative behavior, verifying that the inverse relationship is robust to changes in temperature when three-phonon scattering dominates the thermal conductivity. We would expect the inverse relationship to hold for temperatures higher than 300 K as well, but high temperature thermal conductivity data is not available for the full set of materials we have considered here.

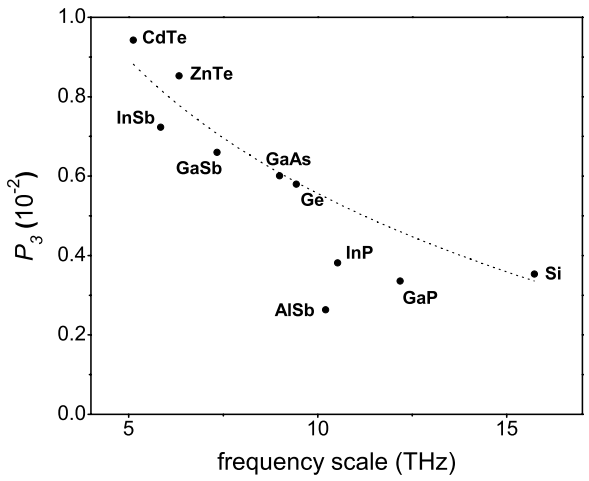

Figure 4. Allowed three-phonon phase space versus frequency scale given by highest calculated optical frequency in a host of semiconductors.

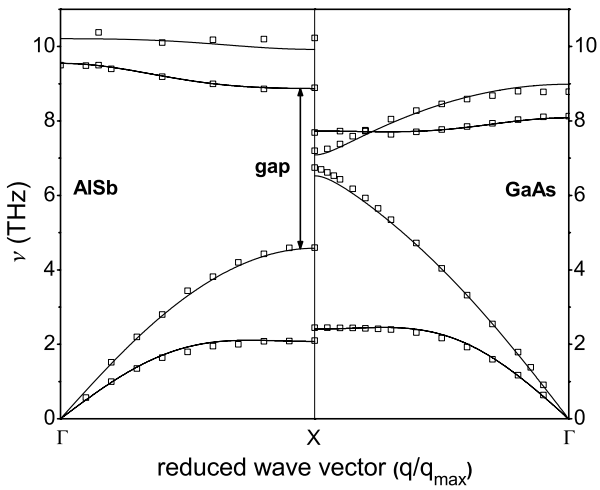

Figure 5. Phonon dispersion curves for AlSb and GaAs illustrating the gap between optic and acoustic modes due to a large mass ratio; neutron scattering data from [18] and [22].

We note that diamond has been left off of figures 2 and 3 because of its exceedingly large thermal conductivity values. Also, unlike all other materials in table 1, diamond has appreciable isotopic impurity scattering in the 150–300 K temperature range; its thermal conductivity is not dominated by phonon–phonon scattering until higher temperature. We also note that the qualitative behavior shown in figures 2 and 3 is also obtained when the phase space due to only umklapp scattering processes is plotted instead of the total three-phonon phase space, P_3. We find that the phase space for umklapp scattering is roughly 55–60% of P_3 in each semiconductor.

It is interesting that the inverse relationship exhibited in figures 2 and 3 occurs in spite of variations in material parameters that are often correlated with the lattice thermal conductivity. For example, the variations in the strength of the anharmonicity, sometimes represented through the Grüneisen constant, are not sufficient to destroy the qualitative trend seen in figures 2 and 3. Only knowledge of the phonon dispersion is required.

The three-phonon phase space depends on the overall frequency scale of the phonon dispersions. To see this, we divide the scattering phase space into four groups of processes according to the number of acoustic (a) and optic (o) phonons involved: (a, a, a), (a, a, o), (a, o, o) and (o, o, o). The (o, o, o) processes are forbidden by the energy conservation condition, while the (a, o, o) processes are severely limited by equation (1) due to the restriction of the momentum space of the acoustic phonon to a small region near the center of the Brillouin zone. The dominant scattering type which contributes most to the three-phonon phase space in the majority of materials is the (a, a, o) group. The (a, a, a) processes also contribute significantly to the phase space, but to a lesser extent than the (a, a, o) processes.

The effect of the frequency scale on the phase space can be seen by examining analytically the three-phonon phase space from the dominant (a, a, o) processes within a Debye–Einstein model. In this model, the acoustic phonons have an isotropic, linear dispersion, $\omega_{ac}(\mathbf{q}) = q v_D$, characterized by a constant velocity, v_D, and Debye cutoff wavevector of magnitude q_D, while the optical phonons have constant frequency, $\omega_{opt}(\mathbf{q}) = \omega_E$. The allowed phase space in the Debye–Einstein model for (a, a, o) scattering, obtained by integrating analytically equations (3), and (4) over the Debye sphere of radius q_D with $j = j' = a$ and $j'' = o$, is:

$$P_3^{(+)}(a, a, o) = \frac{9}{\omega_E}\left[\frac{2\omega_E}{5q_D v_D} - \frac{\omega_E^2}{q_D^2 v_D^2} + \frac{2\omega_E^3}{3q_D^3 v_D^3} - \frac{\omega_E^6}{30q_D^6 v_D^6}\right]. \quad (6)$$

When the dispersion is scaled by a factor β, $\omega_E \to \beta\omega_E$ and $v_D \to \beta v_D$, the phase space is inversely proportional to this scaling factor: $P_3^{(+)}(a, a, o) \to P_3^{(+)}(a, a, o)/\beta$. We find similar scaling behavior occurs for the actual dispersions obtained in the adiabatic bond charge model, which is illustrated in figure 4. As the overall frequency scale, determined by the highest optical frequency, increases from material to material the three-phonon phase space decreases. The same behavior occurs when the scaling is determined by the zone-center acoustic velocities.

For the three III–V materials, AlSb, InP, and GaP, P_3 falls below the general trends in figures 2–4. This anomalous behavior results from the large gap between their acoustic and optic branches, which severely restricts the normally dominant (a, a, o) scattering processes. Figure 5 contrasts the phonon dispersions for the small-gap GaAs and the large-gap AlSb. The large-gap results in part from the substantial mass mismatch between anion and cation, as can be seen from table 1. The phase space reduction can be seen in the two-phonon density of states, $D_j^{(\pm)}(\mathbf{q})$, given in equation (4). The two-phonon density of states, $D_{LA}^{(+)}(\mathbf{q})$, in which a longitudinal acoustic (LA) phonon combines with another acoustic phonon to produce an optic phonon, is shown in figure 6 for two large-gap materials, InP and AlSb, and a small-gap material, GaAs. In GaAs, LA phonons throughout most of the frequency range can contribute to $D_{LA}^{(+)}(\mathbf{q})$. Conversely, in InP and AlSb, only the high-frequency LA phonons have enough energy to combine with another acoustic phonon to create an

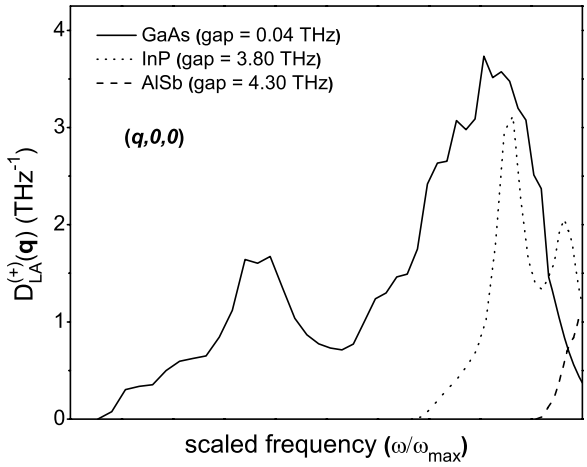

Figure 6. Two-phonon density of states for an LA phonon in the $(q, 0, 0)$ direction for GaAs, InP, and AlSb for which the scattering involves the combination of two acoustic phonons into a higher energy optical phonon. The horizontal axis is the LA phonon frequency scaled by the maximum frequency.

optic phonon, thus severely restricting this scattering channel and reducing the allowed three-phonon phase space. This restriction is reflected in the ratio of (a, a, o) processes to (a, a, a) processes, which in AlSb, InP, GaP and GaAs is 0.03, 0.67, 0.57 and 3.16 respectively. For comparison, values for the energy gap and three-phonon phase space are listed in table 1.

We now consider hypothetically the effect of reducing the energy gap in InP, GaP and AlSb. In this case, the (a, a, o) processes would increase, driving P_3 up, and at the same time this increased scattering would decrease the thermal conductivity. We indicate this hypothetical behavior with the triangles in figure 2, which would place these materials within the general trend.

In the large-gap materials where scattering of the heat-carrying acoustic phonons by optic phonons is significantly reduced, one might question whether four-phonon processes become of comparable significance to three-phonon processes. We have also calculated the phase space for four-phonon scattering in the materials listed in table 1 and found that it is typically 3–4 times larger than P_3. In materials where the (a, a, o) processes are nearly frozen out, the four-phonon phase space is even larger, being, for example, thirteen times larger than P_3 in InP. However, estimates of the room temperature scattering rates for these four-phonon processes are found to be several hundred times weaker than their three-phonon counterparts [5], so despite their less restricted phase space, these higher order processes appear to contribute little to the lattice thermal conductivity around room temperature and below.

Finally, we note that calculation of the three-phonon phase space requires only knowledge of the phonon dispersion, which is determined from the harmonic part of the interatomic forces, as for example expressed in table 2 for the abcm. Once the dispersion is fixed, no adjustable parameters are introduced. In contrast, calculations of the lattice thermal conductivity require as well knowledge of the anharmonic interatomic forces, and simple theories to calculate the thermal conductivity often introduce unphysical approximations and invoke ad hoc fit parameters. Rigorous theoretical approaches to calculate the lattice thermal conductivity that employ exact solutions of the phonon Boltzmann equation have recently been implemented, and accurate microscopic descriptions of the anharmonic interatomic interactions has required *ab initio* approaches [23–27]. Such calculations involve considerable numerical complexity. In this context, the phase space approach presented here can be thought of as providing a qualitative indicator of a material's lattice thermal conductivity.

4. Summary and conclusions

We have calculated the phase space available for three-phonon scattering, P_3, in several of group IV, III–V and II–VI bulk semiconductors. An adiabatic bond charge model was employed to obtain the phonon frequencies. We have shown that the three-phonon phase space varies inversely with the measured lattice thermal conductivity in the temperature range where phonon–phonon scattering dominates. The lack of dependence of this relationship on other material parameters suggests that P_3 could be used to assess qualitatively the thermal conductivities of new materials with known phonon dispersions, where other material parameters have not yet been measured. We have also demonstrated how two features of the dispersion relations, overall frequency scale and the gap between the acoustic and optic branches, affect the phase space for three-phonon scattering and the relationship between this phase space and the lattice thermal conductivity.

Acknowledgment

Acknowledgment is made to the Donors of the American Chemical Society Petroleum Research Fund for partial support of this research.

References

[1] Cahill D G, Ford W K, Goodson K E, Mahan G D, Majumdar A, Maris H J, Merlin R and Phillpot S R 2003 *J. Appl. Phys.* **93** 793
[2] Mahan G D, Sales B and Sharp J 1997 *Phys. Today* **50** 42 Di Salvo F 1999 *Science* **285** 703
[3] Ziman J M 1960 *Electrons and Phonons* (London: Oxford University Press)
[4] Callaway J 1991 *Quantum Theory of the Solid State* (Boston, MA: Academic)
[5] Ecsedy D J and Klemens P G 1977 *Phys. Rev.* B **15** 5957
[6] Weber W 1977 *Phys. Rev.* B **15** 4789
[7] Rustagi K C and Weber W 1976 *Solid State Commun.* **18** 673
[8] Steigmeier E F and Kudman I 1966 *Phys. Rev.* **141** 767
[9] Okubo K and Tamura S 1983 *Phys. Rev.* B **28** 4847
[10] Inyushkin A V, Taldenkov A N, Gibin A M, Gusev A V and Pohl H-J 2004 *Phys. Status Solidi* c **1** 2995
[11] Ozhogin V I, Inyushkin A V, Taldenkov A N, Tikhomirov A V and Popov G E 1996 *JETP Lett.* **63** 490
[12] Wei L, Kuo P K, Thomas R L, Anthony T R and Banholzer W F 1993 *Phys. Rev. Lett.* **24** 3764
[13] Holland M G 1964 *Phys. Rev.* **134** A471
[14] Muzhdaba V M, Nashel'skii A Ya, Tamarin P V and Shalyt S S 1969 *Sov. Phys.—Solid State* **10** 2265

[15] Aliev S A, Nashel'skii A Ya and Shalyt S S 1965 *Sov. Phys.—Solid State* **7** 1287
[16] Slack G A and Galginaitis S 1964 *Phys. Rev.* **133** A253
[17] Slack G A 1972 *Phys. Rev.* B **6** 3791
[18] Strauch D and Dorner B 1990 *J. Phys.: Condens. Matter* **2** 1457
[19] Rajput B D and Browne D A 1996 *Phys. Rev.* B **53** 9052
[20] Press W H, Teukolsky S A, Vetterling W T and Flannery B P 1992 *Numerical Recipes in Fortran* (Cambridge: Cambridge University Press)
[21] Lehmann G and Taut M 1972 *Phys. Status Solidi* b **54** 469
[22] Strauch D, Dorner B and Karch K 1990 *Proc. 3rd Int. Conf. on Phonon Physics (1989)* ed S Hunklinger, W Ludwig and G Weiss (Singapore: World Scientific) p 82
[23] Omini M and Sparavigna A 1996 *Phys. Rev.* B **53** 9064
[24] Omini M and Sparavigna A 1997 *Nuovo Cimento* D **19** 1537
[25] Broido D A, Ward A and Mingo N 2005 *Phys. Rev.* B **72** 014308
[26] Broido D A and Reinecke T L 2004 *Phys. Rev.* B **70** 081310
[27] Broido D A, Malorny M, Birner G, Mingo N and Stewart D A 2007 *Appl. Phys. Lett.* **91** 231922